Etched track profiles for relativistic 7 GeV Silicon and 17.48 GeV Nickel ions in PADC detector: The case study of convex track walls

Michel Fromm, M. Abu-Shady, J.E. E Groetz, E.M. M Awad

Etched track profiles for relativistic 7 GeV Silicon and 17.48 GeV Nickel ions in PADC detector: The case study of convex track walls

M. Fromm*[a], M. Abu-Shady[b], J.E. Groetz[a], E. M. Awad[c]

[a] *Laboratoire Chrono-Environnment, ULR CNRS 6249, Université de Franche-Comté, 16 route de Gray, 25030 Besancon cedex, France.*

[b] *Mathematics and Computer Science Department, Faculty of Science, Menoufia University, Shebin El-Koom, Menoufia 32511 Egypt*

[c] *Physics Department, Faculty of Science, Menoufia University, Shebin El-Koom, Menoufia 32511 Egypt*

Abstract : 650 µm thick PADC foils are exposed to 7 GeV Silicon and 17.48 GeV Nickel accelerated ions at particle fluence of about 1000 cm^{-2}. The relativistic ions passed through the entire thickness of the PADC foils and created latent tracks that were etched sequentially under strong etching conditions (NaOH + ethanol). For each time sequence, etched track profiles were found by carefully polishing the detector edge, and then imaged in order to measure their geometrical parameters (diameter and length). Track wall curvature study allows for better understanding of the physico-chemical interactions undertaken during the etching process. Etched track profiles have the distinctive feature of presenting concave walls near to the track aperture. Such special feature is likely to be due to a depth dependent variation of the bulk etch rate (V_b). This depth dependence is investigated and discussed. A simulation program has been written based on the variational principle, it uses experimentally determined variable V_b and a constant specific track etch rate (V_t). Simulations results are in good agreement with experimental micrographs both qualitatively and quantitatively. Such case study may show promise as a means of fabricating controlled shape pores in polymer membranes.

Keywords : Swift heavy ions, track etching, depth-dependent bulk etch rate, track profiles

Corresponding author:
email address: michel.fromm@univ-fcomte.fr (M. Fromm)

1. Introduction

Since its discovery in 1978(Cartwright et al., 1978; Cassou and Benton, 1978) , chemical etching of nuclear tracks in polyallyl diglycol carbonate (PADC) detector material (often called CR-39^{TM}, its Columbia-Southern Chemical Corporation trade mark) has become a routine process with copious applications worldwide (Espinosa et al., 2013). In use in numerous scientific fields (Henshaw, 2002; Malinowska et al., 2014; Zhou, 2012) PADC is considered as an efficient solid state nuclear track detector (SSNTD); especially due to a wide range of detectable energetic ions, with low or high LET, a low energy threshold (etched tracks of low-LET protons can be observed in PADC) and high sensitivity with inertness towards lower dose electromagnetic noise (He and Price, 1992; Jeong, 2017; Kodaira et al., 2019; Tretyakova et al., 1984; Turek and Dajkó, 2005). Etching process of energetic ion tracks in polymer materials has been studied since long and models allowing track-etch computation to be performed have first been proposed during the early seventies (i.e. 1971-1975) (Fleisher et al., 1975; Henke, 1971. ; Paretzke et al., 1973; Somogyi and Szalay, 1973). Those seminal works have further been developed and improved (Apel et al., 2003; Dörschel et al., 2003; Fromm, 1996, 2005; Fromm et al., 1991; Fromm et al., 1993; Nikezic and Yu, 2004).

Interestingly here, an article published in 1986 by Fujii and Nishimura (Fujii and Nishimura, 1986) got somewhat unnoticed even though, for the first time, the special case of a variable bulk etch-rate was introduced to take account of observations made when long etching times are used to study tracks of energetic nuclei due to cosmic rays. As far as we are aware, the case of a variable bulk etch rate along polymer depth only was considered in details in that particular article. The paper actually describes almost all possible cases meet when nuclear track etching in a polymer is performed; namely i. bulk etch rate (V_b) and specific track etch rate (V_t) both constant (i.e. conical in shape etched track profiles), ii. V_b constant and V_t variable (convex or concave etched track walls depending respectively on an increase or a decrease of the V_t) and iii. V_b variable with depth and Vt constant (i.e. concave or convex etched track walls depending respectively on an increase or a decrease of the Vb with depth), even V_b and V_t both variables can be considered. The model was successfully applied to the case of a depth-dependent V_b and a constant V_t by comparing experimental and calculated etched track openings as well as profiles of a 2 GeV/nucleon iron nucleus track in PADC detector material.

Sagittal etched track sections are extremely important for testing track-etch models as their curvatures are directly linked to the etch-rate ratio V_t/V_b (Fujii and Nishimura, 1986; Yamauchi et al., 2001; Fromm, 2005). Visualization of etched track profiles is not an easy task; it is timeconsuming and sometimes difficult to perform due to the micrometer-scale of single etched tracks; especially when a follow-up (sequential etching) is required. Etched track profiles have first been visualized and analyzed in 1978 (Zamani and Charalambous, 1978), using micrometer cuts. Such track profiles later were used by some of us (Dörschel et al., 2003; Fromm, 1996; Fromm et al., 1991; Fromm et al., 1993), notably to test capabilities and correctness of etching models. Due to the technical evolution of microscopy and improvement of digital tools several attempts have been made to get insight into the etched track morphology, especially to measure detector response functions based on geometric analyses of etched track wall co-ordinates (Awad, 2001; Fromm et al., 2003; Hermsdorf and Hunger, 2009; Vaginay et al., 2001; Wertheim, 2014; Yu et al., 2005). Except the case studies presented by Fujii and Nishimura (Fujii and Nishimura, 1986) (2 GeV/nucleon iron nucleus track) and Awad (Awad, 1999; Awad, 2001) , all other ion track profiles studied in polymer SSNTDs stem from low-Z (Z<6) charged particles with MeV/u or even lower energies.

However, several applications of nuclear track etching in polymers exist where swift heavy ions (SHI) are used as incident projectiles; these include non-exhaustively, high energy nuclear physics (Giacomelli G., 2009; Ota et al., 2011), cosmic ray analysis (Fleisher et al., 1975; Heinrich et al., 1989; Rao Y.V., 1981; Zhou, 2012; Zhou et al., 2006a; Zhou et al., 2006b; Zhou et al., 2010) and track-etched nanoporous polymer membranes and their applications (Apel, 2001; Kaya and Keçeci, 2020; Liu et al., 2018; Wang et al., 2018). These recent years, nanoporous polymeric membrane research has become a very active field with extremely promising perspectives, especially for water filtration and chemical separation in both nano and micrometer scales. In this field, the shape of nanopores plays a central role; a polymeric nanopore model has indeed to be clearly defined and characterized to perform transport experiments and molecular dynamics simulations (Kaya and Keçeci, 2020). A route to fabricate controlled shape pores in polymer membranes, such as for example exaggerated base openings has potential applications in a wide array of fields (Karim et al., 2009; R. Spohr, 1990). The shape of pores and their influence on membrane capabilities was studied by many authors these last decades (Apel et al., 2003; Clochard et al., 2007; Ferain and Legras, 2001; Hadley et al., 2020; Siwy et al., 2003; Tung et al., 2001). Some of us have recently published data in relation with the shape and size of micro-tubes produced by high energy ion irradiation on thick PADC polymer processed in strong etching solution (Awad et al., 2020b). The etched track profiles showed in certain cases new and interesting curvature variations and for the first time, track wall geometry deviated from the shape of simply convex or concave curvature with the appearance of funnel-type etched tracks. In other cases, concave curvature only near to the etched surface was observed. This paper addresses the case of concave etched track walls observed with 7 GeV Si and 17.48 GeV Ni ion tracks etched in strong etching conditions (8 ml of 18 N NaOH+1ml of ethanol) performed at 70°C for sequential time periods varying from 0 to 330 minutes for Si ions and up to 170 minutes for Ni ions. A specific numerical simulation was adopted (Fujii and Nishimura, 1986) and a potential numerical code has been written. This is considered the second trial to simulate high energy ion track since Fujji and Nushimura in 1986. Bulk etch rate variation with depth is intensively investigated since it represents a necessary step to carry out the simulation process and the track wall curvature study as well.

2. Material and methods

2.1. Irradiation, detector material, etching procedure, imaging and parameter measurements

Poly allyl diglycol carbonate PADC polymer SSNTDs of thickness ≈ 650 µm from American Acrylics were used, and irradiated to normal incident high energy ions of 7 GeV Si and 17.48 GeV Ni with particles density ≈ 10^3 particles/cm^2 , for more information, see Table 1.

Ion	E (GeV)	E/n (MeV/n)	R (mm)	dE/dx (KeV/µm)	Irradiation facility
^{28}Si	7.00	250	56.3	73.7	Bevelac, US Berkely
^{58}Ni	17.48	300	40.5	260.9	GSI Germany

Table 1 : Energies, ranges, LETs (SRIM calculations) and irradiation facilities for each of the two ions used in this study (Ziegler et al., 2010).

The detectors were cut perpendicularly to the detector surface into several pieces of area 1 cm^2. Each piece was etched in strong etching solution (Awad et al., 2020a) (8 ml of 18 N NaOH+1ml of ethanol) and the water bath was mounted at 70°C. The track parameters were monitored and recorded at successive etching times. For Ni irradiated samples, etching started with 30 min etching, and then followed by 10 min etching steps. While Si irradiated sample was etched for 60 min to reveal the tracks, then etching successively followed by 15 min etching steps. Removed layer, h is determined experimentally by the change in the thickness of detector sheet over etching time.

Due to etching, cone-shaped etch pits were developed along the latent tracks. Track profiles are then found by carefully polishing the detector edge using a solution of Al_2O_3 powder whose grain size ranges from 0.1 to 5.0 µm. Highly smoothed detector edges were obtained and clear track profile could be seen under the optical microscope after the detector has been mounted on its edge. After each etching, the detector edge was slightly polished at polishing machine to remove the edge roughness. An effort was done to obtain a clear track profile for each ion and optical microphotographs were taken successively for each track profile for investigations and illustrations. The track profile parameters in each etching step were measured. Measurements were carried out using optical microscope (OPTIKA B-1000BF-ALC, Italy) with manual eyepiece micrometer of 0.5 µm step division. The detector material has a good optical transparency leading to good track identification even for tracks situated some micrometers below the edge surface. The track parameters for 1-5 profiles were measured in each etching step and their average was obtained. One of the major drawbacks in track profile technique (TPT) is that only a few numbers of clear tracks are available for measurements. Track opening diameter and track cone length for the followed profiles were recorded following every etching step using a multistage or successive etching process.

Due to etching, the removed layer, h was determined experimentally from thickness change. The cone length, L and the track diameter, D of etched track cone were measured directly as well. The direct track etch rate V_t (h, L) at any point along the ion's trajectory as a function of the etching time, t can be expressed as follows:

$$V_t(h,L)=\frac{L+h}{t} \qquad (1)$$

And detector sensitivity is given by :

$$V(D,L)=\frac{V_t}{V_b}=\tan^{-1}\left(\frac{D/2}{L}\right) \qquad (2)$$

The bulk etch rate is then determined from the above previous equations as:

$$V_b(h,D,L)=\frac{V_t}{V(D,L)}=\frac{\frac{(L+h)}{t}}{\tan^{-1}\left(\frac{D/2}{L}\right)} \qquad (3)$$

Bulk etch rate (Manzoor, 2007) can also be deduced from simultaneous measurement of cone diameter, D and cone length, L of etch-pits caused by relativistic heavy ions as follows:

$$V_b(D,L)=\frac{D^2}{4tL}\left[1+\sqrt{1+\frac{4L^2}{D^2}}\right] \qquad (4)$$

This equation enables to determine V_b at any depth inside the detector. Hence track etch rate, V_t in terms of D, L is then given as follows:

$$V_t(D,L) = V_b \times V = \frac{D^2}{4tL}\left[1+\sqrt{1+\frac{4L^2}{D^2}}\right]\tan^{-1}\left(\frac{D/2}{L}\right) \qquad (5)$$

2.2. Monte Carlo simulations - Energy deposition:

Calculations of LET and radial doses were performed with two computer codes, FLUKA version 2020, from CERN (European Organisation for Nuclear Research) and INFN (Istituto Nazionale di Fisica Nucleare) (Ferrari et al., 2005) and PHITS 3.20 (Particle and Heavy Ion Transport code System) from JAERI (Japan Atomic Energy Research Institute) (Sato et al., 2018). Both have an appropriate description of heavy ion physics at high energy, through fragmentation and evaporation models. The energy cut-off, i.e. minimum energy for which a particle was tracked, was set to 1 keV. Production of secondary particles was also activated, especially for delta electrons, down to 1 keV. In the present study, the ion beam is a pencil beam which interacts with a PADC sample and 10^5 incident ions were considered for every calculation at their nominal energies.

2.3. Track etching simulations:

Etch-pit profiles can be calculated by applying Huygen's principle or the least-time method (Fleischer et al., 1969). Fujii and Nishimura in 1986 derived generalized equations for etch-pit profiles using the variational principle, which is a direct consequence of Huygen's principle (Fujii and Nishimura, 1986). The generalized equations are applicable to the case where neither the bulk nor the track etch rate is constant and if both are constant as well. These equations are thus applicable to the case of varying V_b. However, in the present work, varying V_b and constant V_t was assumed. In order to calculate the shape of the etch pits in the track detector, the depth dependence of V_b is essential to be determined. Hayashi and Doke (1980) pointed out that the dip angle dependence of the etch rate ratio, V_t/V_b, for relativistic particles might be due to a change of V_b with the depth in CR-39 plastic sheets(Hayashi and Doke, 1980). Let us consider the simplest case with a constant Vt and V_b as a brief introduction to the general case with varying V_t and V_b. The coordinate system used is shown in Fig. 1. The x axis is chosen so as to coincide with the trajectory of the charged particle and θ is the ion dip angle.

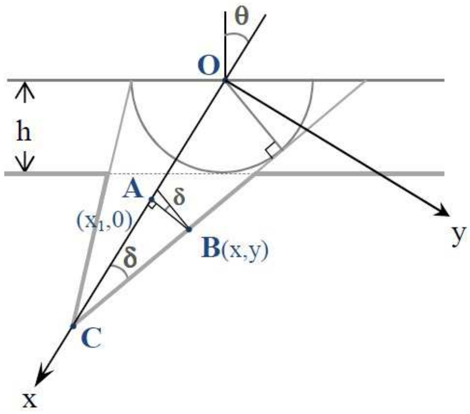

Figure 1 : Geometric representation of an etched track with dip angle θ in the case of a conical in shape model (i.e. both V_b and V_t are constant).

The etching time, t to reach the point B(x,y) on the etch-pit profile is given by :

$$t = \frac{h}{V_b} = \frac{OA}{V_t} + \frac{AB}{V_b} = \frac{x_1}{V_t} + \frac{(x - x_1)}{V_b \sin(\delta)} \qquad (6)$$

where h= V_b*t is the amount of the surface removed during etching time t, δ is the cone angle, x_1 is the coordinate of the point A where the etching path departs from the x axis. The line AB is normal to the etch-pit wall. The value of y expresses as :

$$y = (x - x_1)\cos(\delta) \qquad (7)$$

The cone angle δ depend on the etch rate ratio *sin(δ) = V_b/V_t=1/V*, with V, the detector sensitivity. In the special case where the track rate along the ion track, V_t and the bulk etch rate V_b(Z) as a function of depth inside the detector are known, then the etch-pit profile can be determined numerically by solving the following differential equation:

$$\ddot{y} = (1 + \dot{y}^2)(\dot{y}\cos(\theta) - \sin(\theta))\dot{V}_b / V_t \qquad (8)$$

This equation can be integrated by the Runge-Kuta method if V_b is given as a function of depth. The solution of equation 1 gives the path along which the etching proceeds. The boundary condition needed to solve eq. 1 are:

$$x - x_1 \quad y = y_1 = 0$$

$$\dot{y} = \pm\sqrt{\left(\frac{V_t(x)}{V_b(x_1\cos(\theta))}\right)^2 - 1} \qquad (9)$$

The etch-pit profile, however, cannot be derived from equation (8) alone, because this equation does not contain any information about the etching time. The time, t_{AB} during which the etching reagent proceeds along the path AB is given by:

$$t_{AB} = \int_{x_1}^{x_2} \frac{\sqrt{1+\dot{y}^2}}{V_b(Z)} dx \qquad (10)$$

In (10), the depth is now represented by « Z ». The time t_{AB} expressed in terms of the total etching time, t is as follows:

$$t - t_{OA} = \int_0^1 \frac{dZ}{V_b(Z)} - \int_0^{x_1} \frac{dx}{V_t(x)} \qquad (11)$$

Here we have put h = 1, which can be done without loss of generality because the depth Z can be measured in units of the surface removal h. If we assume a certain value of x_1, the time ($t - t_{OA}$) of equation (11) can be calculated. Then we integrate equation (10), step by step until t_{AB} becomes equal to ($t – t_{OA}$). Integration is performed by the midpoint method using the values y and $\dot{y}$ which are derived by integration of equation (8). The x and y coordinates at this time, $t_{AB} = t - t_{OA}$, are those of a point B on the etch-pit profile (Figure 1). The flow chart of the procedure to derive a etch-pit profile is essentially the same as the one presented by Fujii and Nishimura (Fujii and Nishimura, 1986), except the part concerning integration of equation (10) ; for which the midpoint method was used.

3. Results

3.1. Bulk and track etch-rates.

The procedure for bulk etch rate determination was presented above in details. The complete set of experimental data is presented in Figure 2. This allowed the depth-dependent bulk etch rate $V_b(Z)$ to be determined. A function of the type $1/V_b(Z) = a + b \exp(-Z)$ is needed to implement simulations based on the given differential equation and its boundary conditions (eq 8-11) (Fujii and Nishimura, 1986).

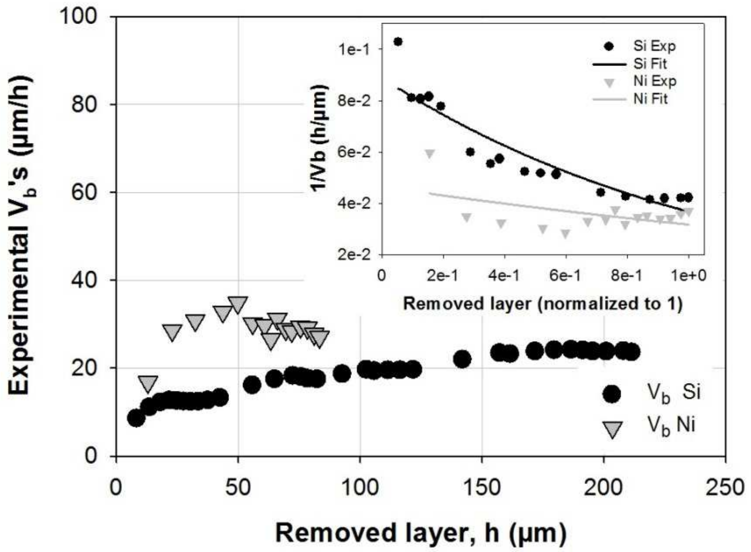

Figure 2 : Experimental V_b as a function of removed layer, h in PADC. The inset shows the $(Vb(z))^{-1}$. Parameters a and b are obtained by fitting the data with the $1/V_b(Z) = a + b \exp(-Z)$ function ; the following best-fits parameter are obtained : a = 0.007 and b = 0.083 for Si and a = 0.017 and b = 0.045. These best fits are presented as full lines in the inset (see legend).

It appears that experimental V_bs exhibit large deviations when comparing Si and Ni data. This is not easy to understand at first sight as V_b is by definition considered ion-independent. Both V_b data sets start in a close vicinity and seem to converge for larger removed layers (> ~100 µm), nevertheless much larger deviations than might be anticipated are observed between 20 and 80 µm removed layers. The Si-exposed detector, for which a larger V_b data set was gathered, is characterized by a quasi-monotonous V_b growth, a very small decrease at large h-values is nevertheless observed. On the contrary, for the Ni-exposed detector a much larger increase of the V_b is measured while for h > 50 µm, a decrease is observed, seeming to converge toward Si data at larger removed layers. The measurements made for very large removed layers (in comparison with few tens of micrometers commonly etched in most of SSNTD applications) within strong etching conditions (ethanol/NaOH) make it visible that structural heterogeneities may exist in PADC material. As noted by others in the case of very long etching times required when studying relativistic ion tracks, there exists a depth-dependence of the V_b (Adams, 1982; Fowler et al., 1980; Portwood et al., 1984; Szilágyi and Somogyi, 1984; Turner et al., 1982). Such depth dependency might be due to undesirable thermal gradients and internal temperature fluctuations in the sheet being cast (Szilágyi and Somogyi, 1984).

Figure 3 presents the V_t determined experimentally based on sequential etching of Si and Ni SHI etched tracks in 650 µm thick PADC. A satisfactory agreement is found when comparing both V_t data sets; namely Vt(h,L) and Vt(D,L) for both studied SHI. It should be noticed that the special behavior of the V_b observed in the range of removed layers from 20 to 80 µm for Ni ions also appears for the measured V_t values (see Figure 3). As V_t measurements made herein depend on the removed thickness, h and thus on the V_b, this is not surprising. As for the specific track etch rate measurements, after a given etching time t, $V_t(h,L) = (L+h)/t$, where L is the etched track length directly measured on the experimental etched track profile. V_t can also be determined using a combination of D and L, where D is the etched track diameter (Awad et al., 2020) and references therein. In a first glance, the specific track etch rates should be envisioned as constant for a fixed SHI energy within given etching conditions. At the high energies used, the Linear Energy Transfert (LET) variations for a given SHI (Si or Ni) passing completely through the PADC detector should be extremely low (see next section). It is therefore likely that the damage rate also remains quasi-constant along the SHI's path, thus the V_t. The contribution from uncertainties in the experimental measurements and the existence of a depth dependency (specific to each used detector) are such that outcome data become a bit remote from those awaited from a strictly constant V_t. In addition, depth dependency of the V_b contributes significantly to the variation of measured V_t data. Obviously, the trend of measured V_t, especially for Ni SHI, is reminiscent of the experimentally determined V_b. V_t's for Si ions increase slowly and monotonously as a function of removed layer as those for Ni ions first increase, then decrease and become saturated at removed layers, h>50 µm. From Figures 2 and 3 one can notice that region between 20-50 µm depth show a kind of instability regarding V_b and V_t mean while beyond >50 µm show stable region for both quantities.

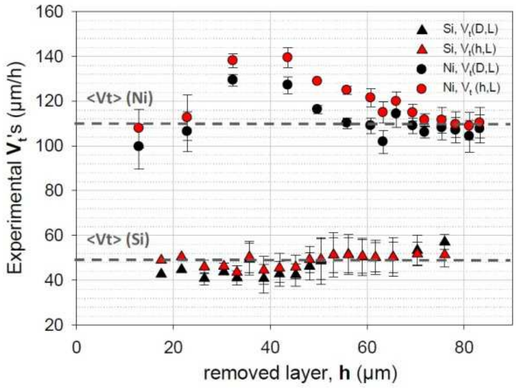

Figure 3: Experimental V_t data as a function of removed layer in PADC for Si and Ni SHI, see text for more information. The dashed lines indicate respectively the average values that were used for etching simulations since V_t is considered constant.

With 7 GeV Si and 17.48 GeV Ni SHI, obtained V_t values lie respectively in the following ranges [40-58] and [100-140] µm/h; calculated average values are respectively 47µm/h and 110 µm/h. These last average values have been used herein for etching simulations based on the least-time method.

3.2. Linear energy transfer and radial dose

Before going into further details concerning etching simulations, the two following specific hypotheses should be checked. First, the observed depth dependency of the V_b could be linked to a cumulative effect of radial dose deposition with depth in the detector. Second, the guess that V_t remains constant can be verified if at least the LET remains itself constant all through the PADC material.

If radial dose deposition expands over large distances, it might be likely that the whole material would suffer degradation and therefore be characterized by variations of the bulk etch rate. The hypothesis we want to test is that radial occupation density profiles of chemical damages could tend to overlap and may thus modulate the bulk etch-rate with a possible depth-dependence. With an ion fluence of 1000 cm^{-2} used with both Si and Ni SHI, it is possible to estimate the radial distance over which a noticeable dose had to be deposited in order to seriously affect the bulk material. Roughly, such radial distance should be of the order of ~ 150 µm to cover 1 cm^2 with 1000 incident SHI. Intuitively, such expansion of the radial dose looks a bit unreasonable, especially because it is well-known that radial dose exhibits a rapid decrease with an increase of the distance to the ion's path (Waligórski et al., 1986). Nevertheless as we are dealing with relativistic ions for which released high energy photons and energetic secondary electrons should have large inelastic mean free paths in condensed matter. It was for example shown that non-relativistic 10 MeV/n Fe ions have radial doses which expand over 4000 nm in water (Awad and Abu-Shady, 2020). It is therefore preferable to estimate the radial extension of dose for the SHI used in this study in order to check those assumptions. The radial doses cumulated all along the 650 µm of the PADC thickness are calculated using the PHITS code (Sato et al., 2018) for the two ions used. We present in Figure 4 the results of these calculations. The cumulative radial dose is determined for the sole ion, for the secondary electrons generated and for both of them (ion + electrons). The general trend observed is that the total cumulative radial dose deposited (ion + electrons) in PADC material starts near to 100 $Gy.ion^{-1}$, then drops down to 10^{-5} – 10^{-4} $Gy.ion^{-1}$ at radial distances of 50 µm. The highest radial doses are approximately deposited in the first 0.4 µm, at these “small” distances the radial doses belong to the range 1-100 $Gy.ion^{-1}$. As far as we are aware, there are no published studies aiming to relate bulk etch rate modifications to SHI radial dose deposition. One study in relation with the effect of gamma ray doses on the V_b when strong etching was used (S. Brahimi et al., 2008) has been published. In that study, PEW etching solutions, namely Potassium hydroxide – ethanol – water was used. PEW has similar etching properties to Sodium hydroxide – ethanol – water mixtures which have been used herein. In the study by Brahimi et al., it is experimentally demonstrated that the increase of the bulk etch rate is significant in the dose range 10^2 – 10^4 Gy and that the higher the increase (%) of ethanol in the PEW solution, the higher the increase of the

V_b. Based on these observations, it is thus unlikely that the 10^3 ions.cm^2 used in the present study would noticeably modify the bulk etch rate of the material.

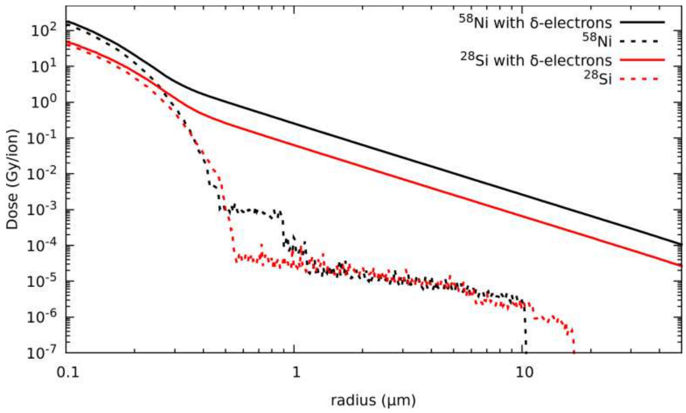

Figure 4: Cumulative radial doses calculated for Si and Ni ions using the PHITS code (Sato et al., 2018).

The observed depth variations of the V_b for long etching times in strong etching conditions should thus rather be linked to structural inhomogeneity within the PADC material as mentioned above, mainly stemming from the PADC casting process (Adams, 1982; Fowler et al., 1980; Portwood et al., 1984; Szilágyi and Somogyi, 1984; Turner et al., 1982). Besides, the noticeable differences observed in Figures 2 & 3 when comparing the experimental V_b and V_t data for PADC material exposed on the one hand to Si and the other to Ni ions are likely to highlight batch-dependent etching properties, especially in the depth range 0- 60 μm.

As for the second hypothesis made which concerned the constant V_t; LETs for each ion used have been computed using PHITS and FLUKA (Ferrari at al, 2005) codes. LET's due to the ion alone, to the δ-electrons and total LETs (ion + electrons) are presented in Table 2.

Ni (17.48 GeV)	Code	Entrance (keV.µm^{-1})	Exit (keV.µm^{-1})
Total	Fluka	380	400
	Phits	340	355
Ion	Fluka	279	280
	Phits	244	249
electrons	Fluka	101	120
	Phits	95	105
Si (7 GeV)			
Total	Fluka	107	112
	Phits	85	88
Ion	Fluka	79	79
	Phits	61	62
electrons	Fluka	28	33
	Phits	24	26

Table 2: Linear energy transfers for 7 GeV Si and 17.48 GeV Ni ions, secondary electrons and ions + electrons as provided by Phits and Fluka codes.

It can be seen from Table 2 that ion LETs at the PADC entrance are in satisfactory agreement with those provided by SRIM calculations (Table 1). Data provided by Phits compared to those from Fluka code are systematically lower, sometimes reaching a difference of the order of 20%. Nevertheless we are here interested in the difference between LETs at the entrance and at the exit of the PADC foil. The general trend is that the difference is extremely low, typically 5%. LET data increase, as may be anticipated, very slowly from one side of the PADC foil (entry) to the other. We can thus state that the assumption of a constant V_t is reinforced.

3.3. Etched track simulations:

Based on a constant V_t = 47 µm/h and a variable V_b of the following analytical form : 1/Vb(Z)= 0.017 + 0.045 exp (-Z), the differential equation and its boundary conditions (Equations 8-11) has been solved numerically and a simulation has been performed for Si etched track profile for 5.5 h. The simulation profile dimensions are then compared with the real profile photograph. Fig. 5-a shows the simulated and the real photograph for 5.5 h superimposed Si profiles. One can see the beauty and the potential of the current code. A scaling factor was obtained and implemented for the whole profiles sequence. Similarly, the simulation has been performed for Ni ion track etched for 170 min using a constant V_t = 110 µm/h and a variable V_b equation: 1/Vb(Z)= 0.007 + 0.083 exp (-Z). Fig. 5-b shows the simulated and the real photograph for 170 min Ni profiles are superimposed and the corresponding scaling factor was obtained. A set of simulations was performed for Si etched tracks sequence and the results are shown in Figure 6. Another etched track profile sequence for Ni tracks was obtained, Fig. 7. In these Figures, simulated etched track profiles have been superimposed to the experimental snapshots ensuring that the scale is kept identical, without any distortion.

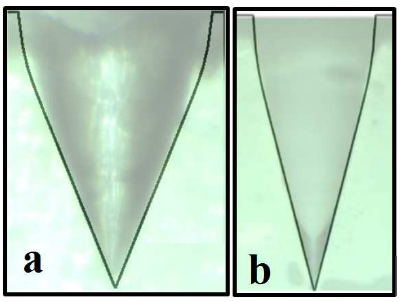

Figure 5: Figure(a) shows both experimental and simulated (black line) Si etched track profile for 5.5 h etching time. Figure (b) is the simulated (black line) and the real microphotograph for 170 min Ni profile.

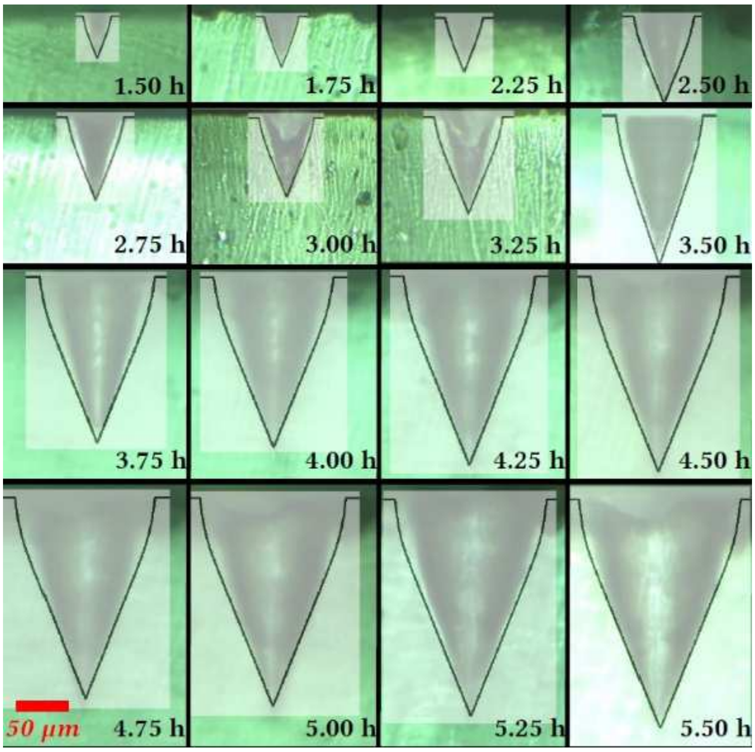

Figure 6: Simulated etched track profiles for 7 GeV Si SHI slowed down in PADC material. Etching times for the sequence appear below each micrograph. The scale of the complete set of simulations is indicated below left.

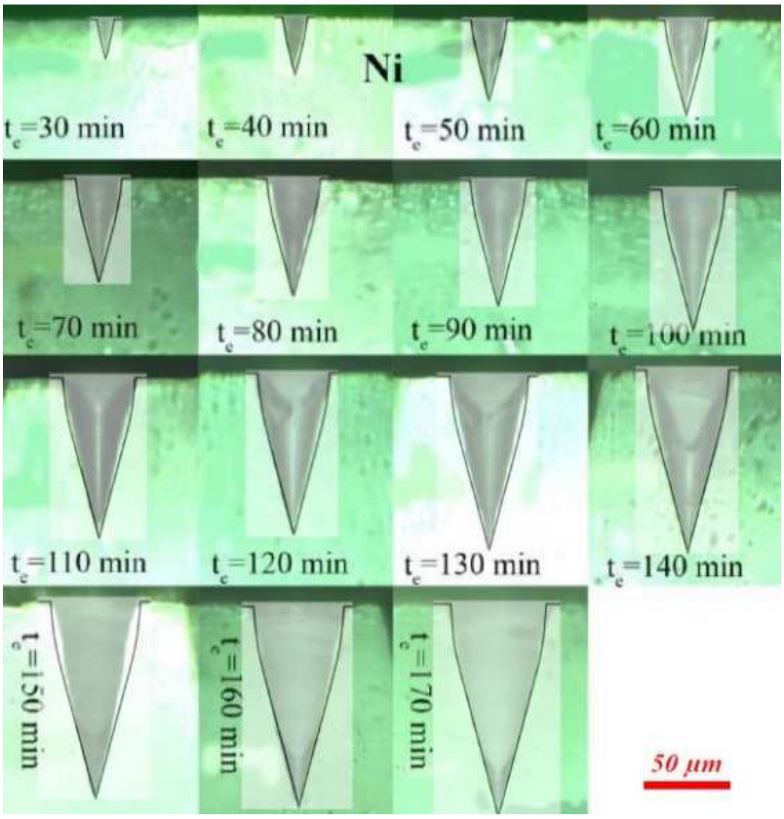

Figure 7 : Simulated etched track profiles for 17.48 GeV Ni SHI slowed down in PADC material. Etching times for the sequence appear below ~~on~~ each micrograph. The scale of the complete set of simulations is indicated right.

A good qualitative and quantitative agreement between simulated track profiles and experimental snapshots is obtained. Some discrepancies can be found but they stem rather from irregularities of the etched track profiles themselves than from computation, most probably due to the difficulty to get a perfect cut of the etched track. It is indeed obvious from Figures 6&7 that the few cases for which the agreement between simulation and experiment is less good are those with rough cuts, namely those for which the ideal profile was partly planed by polishing. The complete sequence of etching for Si and Ni ions also has been simulated; it is presented in Figure 8. On that figure the evolution of the track walls is clearly evidenced, especially concerning the effect of a variable V_b which produces convex track walls near to the track mouth. With a greater etch rate ratio V_t/V_b for Ni than Si, Ni etched tracks look much elongated than Si-ones.

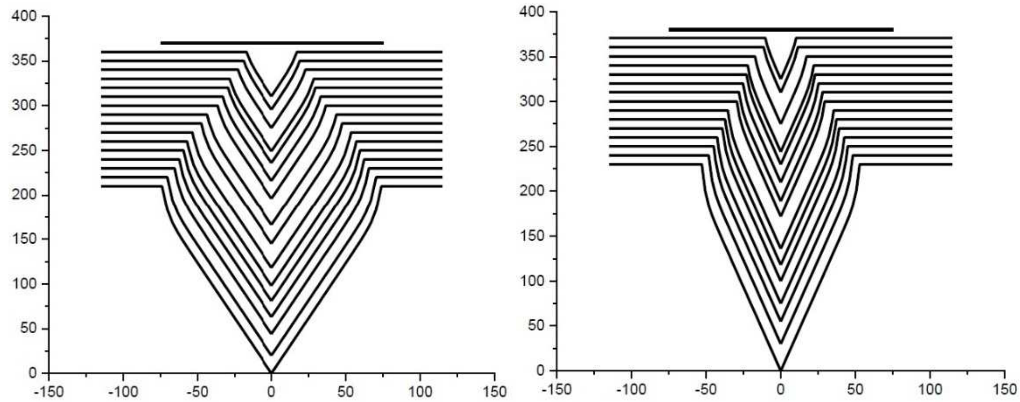

Figure 8: Simulated sequences of track etching for 7 GeV Si SHI (left) and 17.48 GeV Ni SHI (right) for the time steps used in the present study.

The comparison of simulated versus experimental diameters (D) and etched track lengths (L) is presented in Figure 9a for Si ions and in Figure 9b for Ni ions. Concerning Si ions, correlation between simulated and experimental etched track length is acceptable, however, for track diameters, dispersion is observed, especially for the data between 50 and 100 µm. The same remark as below holds, namely that some cuts are not exactly in the sagittal plane of the etched track and therefore deviate from computed ones when measured on the experimental etched track profiles (see Figures 6 and 7 for more details). This problem is obviously less sensible for etched track length measurements. For Ni ions, the correlation looks pretty good for both D and L simulations.

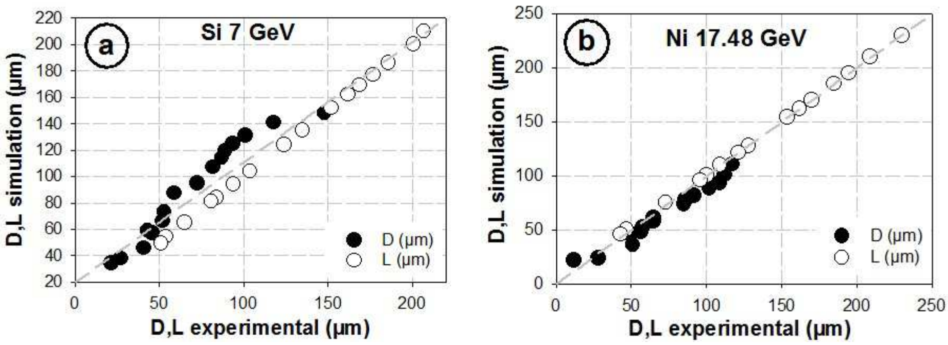

Figure 9: Simulated versus experimental etched track diameters (D) and etched track lengths (L) for, a: 7 GeV Si SHI, b: 17.48 GeV Ni SHI.

For incident SHI which traversed completely the detector, simulations could be performed at any time lower or equal to the time $t_{1/2}$ needed to reach the center of the PADC sheet. When the etching time exceeds the break-through time $t_{1/2}$, both sides are connected and the membrane starts to be permeable through the channels created, see (Awad et al., 2020b) for more details. Geometry and the physical interpretation for nuclear track membranes will be studied soon.

4. Conclusion

A new potential simulation track profile code has been proposed by solving the differential equation suggested by (Fujii and Nishimura, 1986) and its boundary conditions. It allows better understanding and more accurate track development evolution with etching time (depth). It can be used for different track types where V_b and V_t are constant or varying (increasing or decreasing).

Track curvature at a given depth (sequence) is dedicated by V_b and V_t history in the preceding stages. Therefore, deep depth bulk and track etch rate study was carried out. It was found the bulk etch rate, V_b for the two studied ions (Si and Ni) is increasing with depth inside the PADC detector with different rate. Varying V_b history has been incorporated in the calculated track profile through the normalized $1/V_b$ equation.

Information about the physico-chemical process can be deduced from studying the track wall curvature profile. In the present work, the varying V_b and constant V_t have been assumed. Fifteen Si profiles sequence of different etching time and detector depths have been obtained and successfully simulated. Similarly, sixteen Ni profiles were obtained experimentally and simulated. A potential code for track wall curvature expectation at different removed layers (depth) has been obtained.

LET Variations after SHI where slowed down through the PADC membrane have been computed using Fluka and Phits; they are so small that the assumption of a constant V_t is verified. A trial has been given to explain the depth variation of V_b in terms of the secondary electrons produced during the ion pass and the corresponding radial dose distribution was obtained using Fluka and Phits Monte Carlo codes. Based on literature data and Monte Carlo simulations of both codes, the cumulative radial dose deposited all through the PADC foil, we can state that the influence of this radial extension of dose cannot be at the origin of the observed depth dependence of the V_b. The present study provides supplementary presumptions for the case of V_b depth-dependence. This dependence is likely to be due to intrinsic structural heterogeneities of the PADC material which should certainly be created during the casting process of the sheets.

If the model used can be considered valid, then it may also be used for shorter or longer etching times, as soon as the tracks are not over-etched (i.e. when the channels are open). Those aspects of break-through etching and the case of funnel type etched tracks will be treated in a separate publication.

Acknowledgements: The authors are thankful to Ms Eman Bebers for helping and providing some data from her M.Sc Thesis.

References

Adams, J.H., 1982. A curing cycle for detector-quality CR-39, in: Fowler, P.H., Clapham, V.M. (Eds.), Solid State Nuclear Track Detectors. Pergamon, Amsterdam, pp. 145-148.

Apel, P., 2001. Track etching technique in membrane technology. Radiation Measurements 34, 559-566.

Apel, P.Y., Blonskaya, I.V., Orelovitch, O.L., Root, D., Vutsadakis, V., Dmitriev, S.N., 2003. Effect of nanosized surfactant molecules on the etching of ion tracks: New degrees of freedom in design of pore shape. Nuclear Instruments and Methods in Physics Research Section B: Beam Interactions with Materials and Atoms 209, 329-334.

Awad, E.M., 1999. Depth sensitivity of Lexan polycarbonate detector. Radiation Measurements 31, 133-136.

Awad, E.M., 2001. Direct determination of track etch rate and response of CR-39 to normal incidence high-energy heavy ions. Radiation Measurements 33, 855-858.

Awad, E.M., Abu-Shady, M., 2020. Radial dose distribution and effective delta ray radius (Penumbra radius): Determination for some ions passing through water. Nuclear Instruments and Methods in Physics Research Section B 462, 1-9.

Awad, E.M., Hassan, S., Bebers, E., Rammah, Y.S., 2020a. Bulk etch rate for PADC CR-39 at extended concentration range of NaOH mixed with ethanol and etchant viscosity study. Nuclear Inst. and Methods in Physics Research B 464, 45–55.

Awad, E.M., Hassan, S., Bebers, E., Rammah, Y.S., 2020b. Strong etching investigation on PADC CR-39 as a thick track membrane with deep depth profile study. Radiation Physics and Chemistry 177, 109104.

Cartwright, B.G., Shirk, E.K., Price, P.B., 1978. A nuclear-track-recording polymer of unique sensitivity and resolution. Nuclear Instruments and Methods 153, 457-460.

Cassou, R.M., Benton, E.V., 1978. Properties and applications of CR-39 polymeric nuclear track detector. Nuclear Track Detection 2, 173-179.

Clochard, M.C., Wade, T., Wegrowe, J.E., Balanzat, E., 2007. Influence of asymmetric etching on ion track shapes in polycarbonate. Nuclear Instruments & Methods in Physics Research Section B-beam Interactions With Materials and Atoms - Nuclear Instruments and Methods in Physics Research Section B 265, 325-329.

Dörschel, B., Hermsdorf, D., Reichelt, U., Starke, S., 2003. Computation of etched track profiles in CR-39 and comparison with experimental results for light ions of different kinds and energies. Radiation Measurements 37, 573-582.

Espinosa, G., Font, L., Fromm, M., 2013. A review of the developments in nuclear track methodology as published in the proceedings of the International Conference on Nuclear Tracks in Solids from 1990 to 2008. Radiation Measurements 50, 1-6.

Ferain, E., Legras, R., 2001. Pore shape control in nanoporous particle track etched membrane. Nuclear Instruments and Methods in Physics Research Section B: Beam Interactions with Materials and Atoms 174, 116-122.

Ferrari A., Sala P.R., Fassò A. and Ranft J., 2005. Fluka: a multi-particle transport code, CERN 2005 – 10 , INFN/TC 05/11, SLAC – R – 773.

Fleischer, R.L., Price, P.B., Woods, R.T., 1969. Nuclear-Particle-Track Identification in Inorganic Solids. Phys. Rev. 188: 563-7(10 Dec 1969). Medium: X.

Fleisher, R.L., Price, P.B., Walker, R.M., 1975. Nuclear tracks in solids: Principles and applications.

Fowler, P.H., Clapham, V.M., Henshaw, D.L., O'Sullivan, D., Thompson, A., 1980. The Effect of Temperature-Time Cycles in the Polymerisation of CR-39 on the Uniformity of track Response, in: François, H., Massue, J.P., Schmitt, R., Kurtz, N., Monnin, M., Durrani, S.A. (Eds.), Solid State Nuclear Track Detectors. Pergamon, pp. 437-441.

Fromm, M., 2005. Light MeV-ions etching studies in a plastic track detector. Radiation Measurements 40, 160-169.

Fromm, M., Membrey, F., Chambaudet, A., Saouli, R., 1991. Proton and alpha track profiles in CR39 during etching and their implications on track etching models. International Journal of Radiation Applications and Instrumentation. Part D. Nuclear Tracks and Radiation Measurements 19, 163-168.

Fromm, M., Membrey, F., El Rahamany, A., Chambaudet, A., 1993. Principle of light ions micromapping and dosimetry using a CR-39 polymeric detector: Modelized and experimental uncertainties. Nuclear Tracks and Radiation Measurements 21, 357-365.

Fromm, M., Meyer, P., Chambaudet, A., 1996. Ion track etching in isotropic polymer: etched track shape and detection efficiency. Nucl. Instrum. Methods B 107, 337 – 343.

Fromm, M., Vaginay, F., Meesen, G., Chambaudet, A., Poffijn, A., 2003. Watching at the correlation between the specific track-etch rate and the primary physical parameters of the swift ion interaction with the CR-39. Radiation Measurements 36, 93-98.

Fujii, M., Nishimura, J., 1986. Generalized etch-pit equations and their application to analyses of tracks in CR-39 with depth-dependent etching properties. International Journal of Radiation Applications and Instrumentation. Part D. Nuclear Tracks and Radiation Measurements 11, 25-33.

Giacomelli G., T.V., 2009. Nuclear Track Detectors. Searches for Exotic Particles. Physics and Biophysics. Springer., Dordrecht.

Hadley, A., Notthoff, C., Mota-Santiago, P., Dutt, S., Mudie, S., Carrillo-Solano, M.A., Toimil-Molares, M.E., Trautmann, C., Kluth, P., 2020. Analysis of nanometer-sized aligned conical pores using small-angle x-ray scattering. Physical Review Materials 4, 056003.

Hayashi, T., Doke, T., 1980. Characteristics of plastic CR-39 for detection of relativistic cosmic ray heavy nuclei. Nuclear Instruments and Methods 174, 349.

He, Y.D., Price, P.B., 1992. Sensitivity study of CR-39 plastic track detectors. International Journal of Radiation Applications and Instrumentation. Part D. Nuclear Tracks and Radiation Measurements 20, 491-494.

Heinrich, W., Wiegel, B., Ohrndorf, T., Bücker, H., Reitz, G., Schott, J.U., 1989. LET spectra of cosmic-ray nuclei for near earth orbits. Radiation research 118, 63-82.

Henke, R.P., Benton, E.V., 1971. . On geometry of tracks in dielectric nuclear track detectors. Nucl. Instrum. Methods 97, 483－489.

Henshaw, D.L., 2002. Applications of CR-39 nuclear track detector in medicine and technology. Physics in Technology 13, 266.

Hermsdorf, D., Hunger, M., 2009. Determination of track etch rates from wall profiles of particle tracks etched in direct and reversed direction in PADC CR-39 SSNTDs. Radiation Measurements 44, 766-774.

Jeong, T.W., Singh, P.K., Scullion, C. et al. , 2017. CR-39 track detector for multi-MeV ion spectroscopy. Sci Rep 7.

Karim, S., Ensinger, W., Mujahid, S.A., Maaz, K., Khan, E.U., 2009. Effect of etching conditions on pore shape in etched ion-track polycarbonate membranes. Radiation Measurements 44, 779-782.

Kaya, D., Keçeci, K., 2020. Review—Track-Etched Nanoporous Polymer Membranes as Sensors: A Review. Journal of The Electrochemical Society 167, 037543.

Kodaira, S., Kitamura, H., Kurano, M., Kawashima, H., Benton, E.R., 2019. Contribution to dose in healthy tissue from secondary target fragments in therapeutic proton, He and C beams measured with CR-39 plastic nuclear track detectors. Scientific Reports 9, 3708.

Liu, F., Wang, M., Wang, X., Wang, P., Shen, W., Ding, S., Wang, Y., 2018. Fabrication and application of nanoporous polymer ion-track membranes. Nanotechnology 30, 052001.

Malinowska, A., Jaskóła, M., Korman, A., Szydłowski, A., Kuk, M., 2014. Characterization of solid state nuclear track detectors of the polyallyl-diglycol-carbonate (CR-39/PM-355) type for light charged particle spectroscopy. The Review of scientific instruments 85, 123505.

Manzoor, S., 2007. Improvements and calibrations of nuclear track detectors for rare particle searches and fragmentation studies.

Nikezic, D., Yu, P., 2004. Formation and growth of tracks in nuclear track materials. Materials Science & Engineering R-reports - MAT SCI ENG R 46, 51-123.

Ota, S., Yasuda, N., Sihver, L., Kodaira, S., Kurano, M., Naka, S., Ideguchi, Y., Benton, E.R., Hasebe, N., 2011. Charge resolution of CR-39 plastic nuclear track detectors for intermediate energy heavy ions. Nuclear Instruments and Methods in Physics Research Section B: Beam Interactions with Materials and Atoms 269, 1382-1388.

Paretzke, H.G., Benton, E.V., Henke, R.P., 1973. On charge particle evolution in dielectric track detectors and charge identification through track radius measurement. Nuclear Instruments and Methods B 108, 73-80.

Portwood, T., Turner, T.W., Fews, A.P., 1984. Kinetics and control of polymerising CR-39. Nuclear Tracks and Radiation Measurements (1982) 8, 155-158.

R. Spohr, 1990 Ions Tracks and Microtechnology. Principles and Application. Friedr. Vieweg&Sohn Verlegsgschaft mbH, Braunschweig.

Rao Y.V., D.A., Hagan M.P., Filz R.C., 1981. CR-39 Plastic Track Detector Experiment for Measurement of Charge Composition of Primary Cosmic Rays. International Astronomical Union / Union Astronomique Internationale (Symposium No. 94 Jointly with International Union of Pure and Applied Physics Held in Bologna, Italy, June 11 – 14, 1980),, Springer, Dordrecht.

Sato T., Iwamoto Y., Hashimoto S., Ogawa T., Furuta T., Abe S-I., Kai T., Tsai P-E., Ratliff H.N., Matsuda N., Iwase H., Shigyo N., Sihver L. and Niita K., 2018. Features of Particle and Heavy Ion Transport code System (PHITS) version 3.02, J. Nucl. Sci. Technol. 55, 684-690.

Siwy, Z., Apel, P., Dobrev, D., Neumann, R., Spohr, R., Trautmann, C., Voss, K., 2003. Ion transport through asymmetric nanopores prepared by ion track etching. Nuclear Instruments and Methods in Physics Research Section B: Beam Interactions with Materials and Atoms 208, 143-148.

Somogyi, G., Szalay, S.A., 1973. Track-diameter kinetics in dielectric track detectors. Nuclear Instruments and Methods 109, 211-232.

Szilágyi, S., Somogyi, G., 1984. Calculation of thermal effects occuring during the manufacture of CR-39 sheets. Nuclear Tracks and Radiation Measurements (1982) 8, 171-174.

Tretyakova, S.P., Borcea, C., Kalpakchieva, R., 1984. The use of CR-39 plastic detector for the detection and identification of ions with $2 \leqslant Z \leqslant 5$. Nuclear Instruments and Methods in Physics Research 221, 371-377.

Tung, K.-L., Chang, Y.-L., Chuang, C.-J., 2001. Effect of Pore Morphology on Fluid Flow through Track-Etched Polycarbonate Membrane. Tamkang Journal of Science and Engineering 4.

Turek, K., Dajkó, G., 2005. Angular response of CR-39 to relativistic heavy ions and high-energy protons. Radiation Measurements 40, 367-370.

Turner, T.W., Clapham, V.M., Fews, A.P., Henshaw, D.L., 1982. On the Qquantitative Analysis and Effects of Iinternal Temperature Fluctuations During Cure of the Polycarbonate CR-39, in: Fowler, P.H., Clapham, V.M. (Eds.), Solid State Nuclear Track Detectors. Pergamon, Amsterdam, pp. 141-144.

Vaginay, F., Fromm, M., Pusset, D., Meesen, G., Chambaudet, A., Poffijn, A., 2001. 3-D Confocal microscopy track analysis: a promising tool for determining CR-39 response function. Radiation Measurements 34, 123-127.

Waligórski, M.P.R., Hamm, R.N., Katz, R., 1986. The radial distribution of dose around the path of a heavy ion in liquid water. International Journal of Radiation Applications and Instrumentation. Part D. Nuclear Tracks and Radiation Measurements 11, 309-319.

Wang, P., Wang, M., Liu, F., Ding, S., Wang, X., Du, G.H., Liu, J., Apel, P., Kluth, P., Trautmann, C., Wang, Y., 2018. Ultrafast ion sieving using nanoporous polymeric membranes. Nature Communications 9.

Wertheim, D.a.G., G., 2014. Application of confocal microscopy for surface and volume imaging of solid state nuclear track detectors. Journal Of Microscopy 254(1), pp. 42-46.

Yamauchi, T., Ichijo, H., Oda, K., Doerschel, B., Hermsdorf, D., Kadner, K., Vaginay, F., Fromm, M., Chambaudet, A., 2001. Inter-comparison of geometrical track parameters and depth dependent track etch rates measured for Li-7 ions in two types of CR-39. Radiation Measurements 34, 37-43.

Yu, K.N., Ng, F.M.F., Nikezic, D., 2005. Measuring depths of sub-micron tracks in a CR-39 detector from replicas using Atomic Force Microscopy. Radiation Measurements 40, 380-383.

Zamani, M., Charalambous, S., 1978. On the shape of etched tracks in SSNT detectors. Nuclear Track Detection 2, 227-231.

Zhou, D., 2012. CR-39 plastic nuclear track detectors in physics research. Hauppauge, N.Y.: Nova Science Publishers.

Zhou, D., O'sullivan, D., Semones, E., Weyland, M., 2006a. Charge spectra of cosmic ray nuclei measured with CR-39 detectors in Low Earth Orbit. Nuclear Instruments and Methods in Physics Research Section A: Accelerators, Spectrometers, Detectors and Associated Equipment 564, 262-266.

Zhou, D., O’Sullivan, D., Flood, E., 2006b. Radiation field of cosmic rays measured at aviation altitudes by CR-39 detectors. Advances in Space Research 37, 1218-1222.

Zhou, D., Semones, E., Guetersloh, S., Zapp, N., Weyland, M., Benton, E.R., 2010. The experimental and simulated LET spectrum and charge spectrum from CR-39 detectors exposed to irons near CRaTER at BNL. Radiation Measurements 45, 916-922.

Ziegler, J. F., Ziegler M.D., Biersack J.P., 2010. SRIM – The stopping and range of ions in matter (2010), Nuclear Instruments and Methods in Physics Research Section B: Beam Interactions with Materials and Atoms, Volume 268, Issues 11–12, 1818-1823.